ELSEVIER

Intermetallics 8 (2000) 143–150

Intermetallics

Solubility of boron in $Mo_{5+y}Si_{3-y}$

J.J. Huebsch, M.J. Kramer*, H.L. Zhao, M. Akinc

Ames Laboratory and Department of Materials Science and Engineering, Iowa State University, Ames, IA 50011 USA

Received 20 May 1999; accepted 10 August 1999

Abstract

Using X-ray analysis, optical microscopy, chemical analysis, and electron probe microanalysis (EPMA) it has been determined that the level of boron solubility in $Mo_{5+y}Si_{3-y}$ at 1800°C reaches a maximum value of approximately 2 at% in a narrow region within the homogeneity range of $-0.08 \leqslant y \leqslant 0.04$. Both the B doped and undoped $Mo_{5+y}Si_{3-y}$ (T1) have the tetragonal W_5Si_3 crystal structure, which corresponds to the I4/mcm space group. Within the single phase $Mo_{5+y}Si_{3-y}B_x$ (T1) region there is a contraction in the lattice volume with increasing boron concentration while there is an increase in cell volume with an increase in Mo:Si ratio. © 2000 Elsevier Science Ltd. All rights reserved.

Keywords: A. Silicides

1. Introduction

Previous work by Meyer et al. [1–3] showed that the addition of as little as 1 wt% (~6.5 at%) boron results in dramatic increases in oxidation resistance in alloys of Mo–Si–B over single phase $Mo_{5+y}Si_{3-y}$. In addition, the boron-doped materials possess creep resistance comparable to that of undoped $Mo_{5+y}Si_{3-y}$ [2]. However, all of these samples were multi-phase, making it impossible to determine the effects that individual phases had on properties such as creep and oxidation resistance. In all of the alloys that possessed good creep strength and oxidation resistance the primary matrix phase was T1 ($Mo_{5+y}Si_{3-y}B_x$). This work also suggested that the level of boron solubility in the T1 phase was lower than previously reported by Nowotny [4]. In order to establish the effect of boron doping on the physical properties of the T1 phase, the solubility field needs to be accurately determined.

Nowotny et al. first studied the Mo–Si–B system during his research into the stabilizing effects of small dopant atoms, such as B, C, O and N, on the crystal structure of $Mo_{5+y}Si_{3-y}$ [4–6]. Their work on the Mo–Si–B system led to the generation of the 1600°C isotherm (Fig. 1). Nowotny and his co-workers prepared their samples by arc melting elemental powder compacts. However, they employed fairly low purity starting materials, as low as 83% boron for some of the samples. Elemental powder compacts were sintered under a hydrogen blanket at 1200°C for 12 h before arc melting under argon. The resulting arc-melted buttons were then annealed in argon at 1600°C for 12 h. Using X-ray diffraction analysis and optical microscopy they estimated the level of boron solubility in the T1 phase to be about 4.5–5 at%.

Although Nowotny's group never produced a single phase T1 material, they did notice a contraction in the measured lattice parameters of T1 with increasing boron content. Using a sample that contained approximately 10 vol% MoB as a second phase, they determined the lattice parameters of the T1 phase to be $a = 9.62$ Å and $c = 4.87$ Å. These lattice values are significantly lower than that reported in the JCPDS data for nominally stoichiometric Mo_5Si_3, which lists lattice parameters $a = 9.648$ Å and $c = 4.914$ Å. They assumed that boron was either replacing silicon in the lattice or that boron was entering into silicon vacancies within the lattice for the Mo rich composition.

The primary purpose of the current study is to determine the boundary of the single phase $Mo_{5+y}Si_{3-y}B_x$ (T1) region and to assess the effect of boron concentration and Mo:Si ratio on the lattice parameters. In order to insure that thermodynamic equilibrium has been reached, due to sluggish diffusion in this system, the solubility range was determined at 1800°C rather than 1600°C.

* Corresponding author. Tel.: +1-515-294-0276.

0966-9795/00/$ - see front matter © 2000 Elsevier Science Ltd. All rights reserved.
PII: S0966-9795(99)00082-5

2. Experimental procedure

A series of compositions around and within the T1 ($Mo_{5+Y}Si_{3-Y}B_x$) region proposed by Nowotny have been prepared (Table 1). The starting materials used were 99.999% lump silicon supplied by Alfa Aesar, 99.95% lump boron supplied by CERAC, and 99.95% molybdenum rod manufactured by CMC Industries. Starting materials were weighed out to the nearest hundredth of a gram before being arc-melted in a non-consumable tungsten electrode arc-furnace using a zirconium getter. Samples were melted three to five times each to ensure homogeneity. Typical sample size was on the order of 45 g.

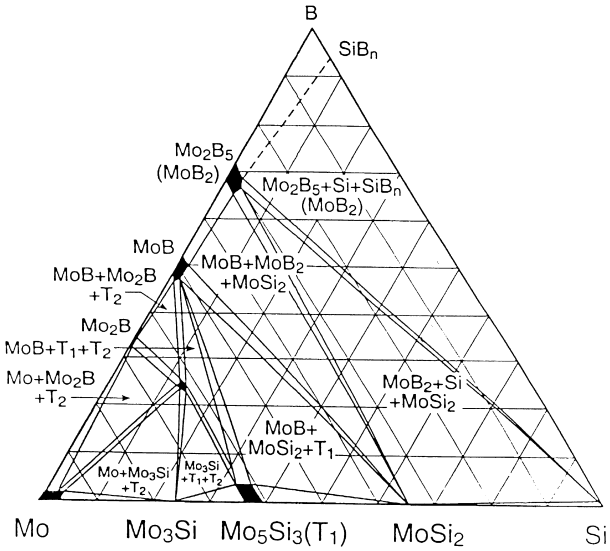

Fig. 1. 1600°C Isotherm of Mo–Si–B system [4].

Powder processing was done inside an argon filled glove box with an oxygen content <0.65 ppm in an effort to keep impurity levels as low as possible. The arc-melted buttons were ground in an impact mill (SPEX® Model 8000) using a tungsten carbide lined vial and 0.5 wt% Dow Methocel™ as a grinding aid. Powders were acid brushed through a −635 stainless steel sieve, with a nominal opening size of 20 μm, and pressed into pellets using a 12.5 mm tungsten carbide lined die at 138 MPa. Removal of the grinding aid from the pellets was accomplished by heating the specimens on a tantalum plate in a tube furnace under flowing high purity argon. Titanium sponge was used as a getter for any residual oxygen or nitrogen impurities in the gas. A heating rate of 3°C/min to 1000°C was used and was held at the temperature for 3 h before being cooled at a

Table 1
Starting compositions used in this study compared to chemical analysis after arc-melting

Sample ID	Initial compostion (at%)			Wt loss (%)	Bulk chemical analysis				
					ICP (at.%)			IGF (ppm)	
	Mo	Si	B		Mo	Si	B	C	O
L	60.0	40.0		0.01	57.9	42.1			
P	60.6	39.4		0.05	59.71	40.3			
M	61.5	38.5		0.02	60.6	39.4			
N	62.5	37.5		0.05	61.1	38.9			
O	63.8	36.2		0.08	62.7	37.3			
Z	61.3	38.2	0.5	0.04	65.5	34.2	0.4		
V	63.0	36.5	0.5	0.15	61.2	38.4	0.5		
ψ	60.2	38.8	1.0	0.02	65.7	33.3	1.0		
λ	61.1	37.9	1.0	0.06	66.3	32.9	0.8		
C	61.7	37.3	1.0	0.06	60.4	38.8	0.9		
δ	62.5	36.5	1.0	0.04	67.2	31.9	1.0		
U	62.8	36.3	1.0	0.02	67.4	31.8	0.8		
Q	63.3	35.7	1.0	0.15				95	147
W	60.1	38.2	1.7	0.06	58.9	39.6	1.5		
A	61.3	37.0	1.7	0.26	60.2	38.3	1.6		
D	62.0	36.3	1.7	0.02				23	182
F	63.5	34.8	1.7	0.04				50	141
B	60.8	37.5	1.8	0.09	59.7	38.7	1.6		
Y	61.0	37.0	2.0	0.04				16	166
I	62.3	35.8	2.0	0.02	60.4	37.8	1.9		
X	61.0	36.5	2.5	0.03				85	174
R	61.0	36.0	3.0	0.03				20	155
J	61.8	35.2	3.0	0.03	60.3	36.9	2.9		
K	60.8	35.4	3.8	0.01				118	154
T	60.2	34.8	5.0	0.07	58.7	36.8	4.5		
Binary 1	46.0	54.0							
Binary 2	70.0	30.0							

rate of 5°C/min to room temperature. Pellets were then sintered at 1800°C under flowing high purity argon. Pellets were placed vertically in a tantalum box, covered with a tantalum lid, and heated at 20°C/min to 1800°C, held for 48 to 72 h, and then cooled at a rate of 5°C/min to room temperature. From the arc-melted button, all the way to the sintered pellet, the materials were processed in an argon atmosphere and were never exposed to air at any time.

The resulting sintered pellet was then cut into three sections using a Struers Accutom-5 with a diamond cut-off wheel. The bottom third of the pellet, which was in contact with the tantalum box, was mounted for optical microscopy, the middle section was used for chemical analysis, and the top third was used for XRD. X-ray powder samples were prepared by grinding the top section of the sintered pellet in air using a SPEX® mill. The powder was then acid brushed through a −635 mesh stainless steel sieve.

X-ray data was collected with a Scintag XDS 2000 diffractometer using a 0.03° step scan with a count time of 2 s. Powder samples were mounted in a single crystal silicon holder and scans were typically run from $2\theta = 10$–$130°$. Single crystal Si was used as an internal standard for some of the samples. Rietveld refinement of the data was performed using G.S.A.S (general structure analysis system) [7] to determine the fraction of phases present and the lattice parameter for the T1 phase. Peak profile coefficients, thermal parameters, specific atom sites, and lattice parameters were varied to get the best numerical fit for the X-ray data.

Optical microscopy samples were prepared by cold mounting the bottom section of the sintered pellet in epoxy and wet polishing down to 0.05 μm alumina. Samples were then viewed under an Olympus optical microscope (model BH3) as well as a JEOL 6100 scanning electron microscope.

Chemical analysis was performed on the middle section of the sintered pellet. Molybdenum, silicon, and boron concentrations were determined using an inductively coupled plasma atomic emission spectrometer (ICP-AES). Carbon impurities were measured by the combustion method using a Horiba Model EMIA-520 Carbon analyzer, and oxygen and nitrogen levels were found by inert gas fusion in a Leco TC-436 nitrogen and oxygen determinator. Accuracy levels given for the chemical analysis are (3 wt% (relative) for ICP on Mo, Si and B, ± 2.6 wt% (relative) for oxygen and nitrogen, and ±2 wt% (relative) for carbon.

EPMA data were collected using an ARL microprobe operating at 15 kV accelerating voltage and a beam current of 20 nA. The count rates on pure element standards were approximately 3150 cps for $Mo_{1\alpha}$ (PET crystal) and 2900 cps for $Si_{k\alpha}$ (ADP crystal). Raw counts were corrected for deadtime, drift in beam current, and background. The matrix (ZAF) correction is discussed below.

3. Discussion

Fig. 2 shows the experimentally determined single-phase T1 region at 1800°C. The dashed line represents the T1 region from the Nowotny 1600°C diagram as a point of reference. The shaded region is based on EPMA results for the Mo:Si while B solubility limit was determined from single phase samples based on XRD and initial starting composition. The work in this study was carried out at 1800°C, rather than 1600°C, in an effort to achieve thermodynamic equilibrium, which may not have been reached at 1600°C, as discussed in more detail below.

The bulk chemical analysis results tended to show slightly lower Mo and slightly higher Si values than expected for most of the compositions. Commercially available single phase $Mo_{5+y}Si_{3-y}$ and $MoSi_2$ (CERAC, Milwaukee, WI) were then used for chemical analysis as a comparison for our samples. Chemical analysis for the commercial samples followed the same trend of having low Mo and high Si values. The analysis showed 58.7 at% Mo and 41.3 at% Si for the Mo_5Si_3, and 30.69 at% Mo with 69.31 at% Si for the $MoSi_2$. Comparing these to known values from the phase diagram, 60–62.5 at% Mo and 37.5–40 at% Si for $Mo_{5+y}Si_{3-y}$ and 33.3 at% Mo with 66.7 at% Si for $MoSi_2$, indicates that the chemical analysis results are somewhat inaccurate. The inaccuracies most likely arose due to difficulty in dissolving the silicides in HF prior to analysis.

The level of uncertainty for the chemical analysis determinations (± 3 wt% relative) are often larger than the differences between the individual samples so the chemical analysis should only be used as a guide. Because this work was done on such a small area of the phase diagram, weight losses were the best method of controlling the compositions. It was important to keep impurity levels as low as possible in order to minimize their effects on boron solubility, particularly carbon which can stabilize the hexagonal Mn_5Si_3 structure. Also, any oxygen present in the material could lead to the formation of silica and thus alter the overall composition of the sample by creating Mo rich $Mo_{5+y}Si_{3-y}$. For these reasons, ICP was no longer performed while IGF was found to be a good guide for tracking quality control of the arc-melting process. The light element impurity levels found in the samples are low enough that they should not significantly influence the level of B solubility (Table 1). However, there is uncertainty in the Mo:Si after long annealing above 1410°C, where SiO begins to vaporize.

The microstructure of the buttons varied extensively from the bottom to top. The grain size of the button on the Cu hearth was 10–100 μm but coarsened rapidly to rather large dendrites, as much as 2 mm in diameter, at the top. Voids and cracks were common. The coarse grains and large solidification features caused concern in being able to achieve chemical equilibrium in these

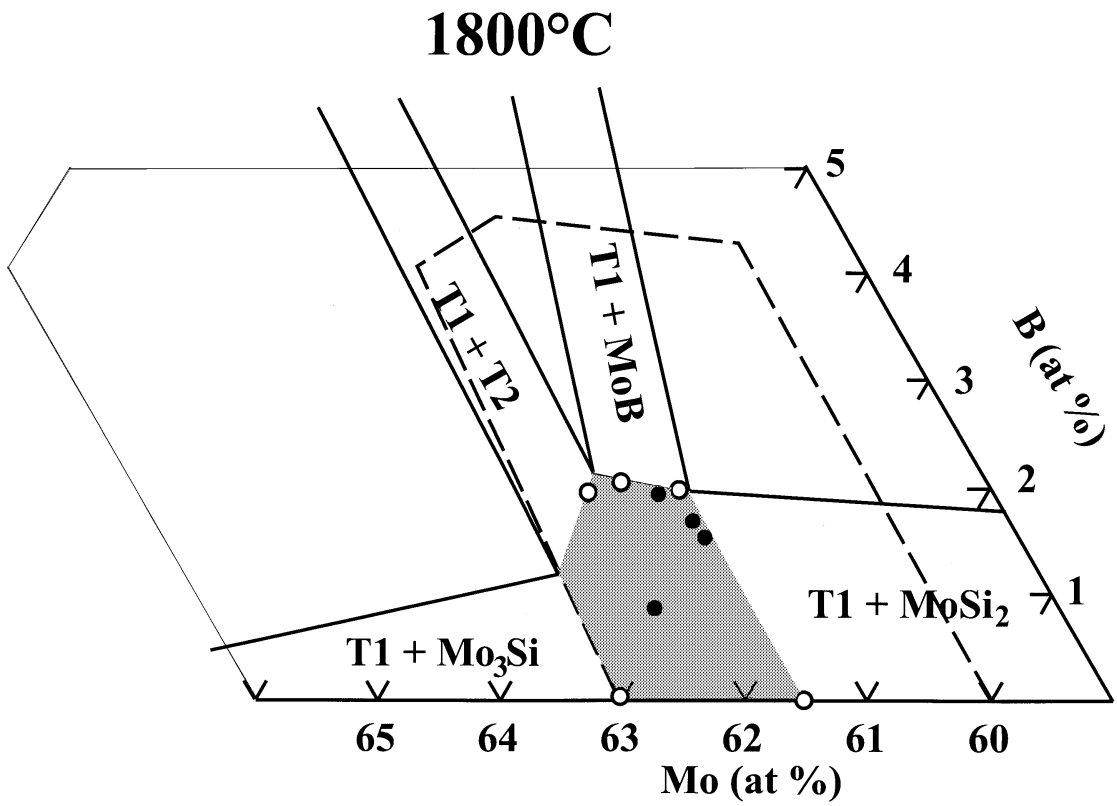

Fig. 2. Experimentally determined T1 region at 1800°C.

samples. In order to determine annealing time necessary to achieve equilibrium, the same arc-melted buttons were annealed at 1800°C for various times. Initially there was concern that the samples would react with the Ta support. However, as evidenced by visual inspection, there appeared to be very little reaction between the samples and the Ta even after as long as 92 h at 1800°C. The sintered pellets did not show a reaction surface and the pellets were easily removed. Sample B was used for the kinetic study, since its initial composition was near the center of the T1 phase field. X-ray pattern of the as quenched arc-melted sample B was found to have a small amount of $MoSi_2$ present (Fig. 3). Pieces of the button were annealed at 1800°C for 2 h and it was found that the disilicide phase, initially present in sample B, disappeared (Fig. 4). All samples were then processed at 1800°C for 2 h then X-rayed. However, numerous samples showed phases not in equilibrium according to the ternary diagram. For example, sample K had T1, MoB, T2, and hexagonal $Mo_{5+y}Si_{3-y}$. After a second higher temperature annealing at 1900°C for 5 h, it was apparent that the hexagonal $Mo_{5+y}Si_{3-y}$ and T2 phases were disappearing (Fig. 5), but were not entirely gone. This indicated that thermodynamic equilibrium was still not being reached. Others [8,9] have experienced similar problems reaching equilibrium with this refractory system.

In order to balance volitization of Si yet maintain high diffusivity, it was decided to powder process the arc-melted buttons in an inert atmosphere and anneal the samples for 48 h at 1800°C. After 48 h at 1800°C sample K showed two phases, T1 and MoB. The hexagonal $Mo_{5+y}Si_{3-y}$ and T2 phases had disappeared and were not detectable using XRD or SEM (Fig. 6). Grinding the arc-melted buttons dramatically cuts the diffusion path for this system since arc-melted buttons have grain sizes of the order of 100 μm or larger while ground powders average starting particle size is less than 10 μm. Due to the high degree of cracking in arc-melted buttons, the geometric density of the sintered pellet is higher, thus aiding in diffusion once sintering has occurred.

After annealing all of the samples for 48 h at 1800°C, X-ray patterns were used to determine equilibrium phase assemblages. It was found that the equilibrium phase assemblages around T1 shown on the Nowotny diagram still hold true at 1800°C (Table 2). However, based upon starting compositions, the single phase T1 region was found to be much smaller than that shown on the Nowotny 1600°C isotherm. This finding corroborates with the observations made by Nunes et al. [8] in which the authors reported that the solubility regions of the boride phases, shown on the phase diagram in Fig. 1, are much smaller than originally claimed by Nowotny.

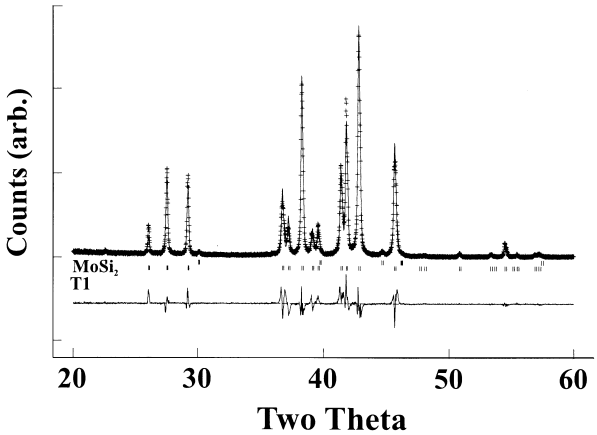

Fig. 3. Rietveld refined XRD of the as quenched arc-melted button B. Measured intensity for each step is a '+' and the solid line is the theoretically calculated pattern using GSAS. Tick marks identify expected diffraction peaks for each phase listed below the scan. A plot of the difference between the observed and calculated XRD patterns is shown below the XRD scan.

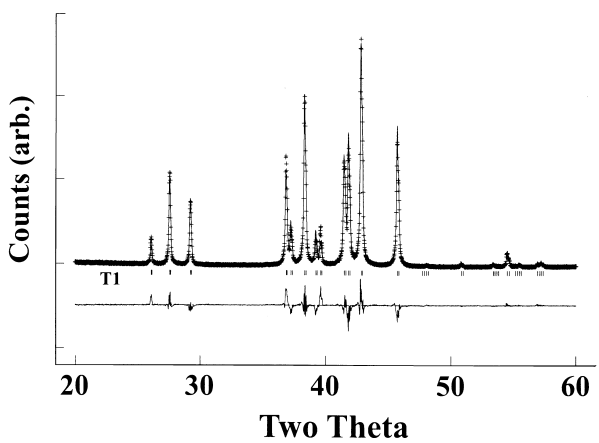

Fig. 4. Rietveld refined XRD of the arc-melted button B annealed 2 h at 1800°C. Note the $MoSi_2$ is no longer observed.

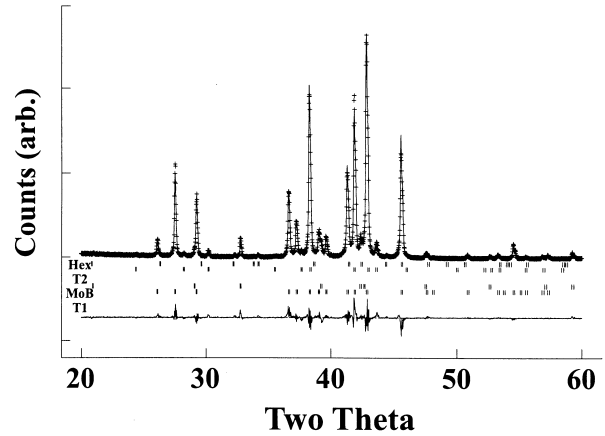

Fig. 5. Rietveld refined XRD of sample K annealed for 5 h at 1900°C. The four phases indicated (hexagonal Mo_5Si_3, T1, T2 and MoB) clearly violate thermodynamic equilibrium.

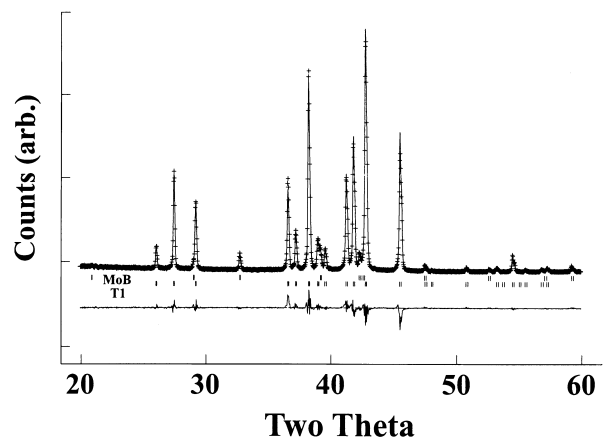

Fig. 6. Rietveld refined XRD of sample K powder processed and annealed 48 h at 1800°C showing the expected phases based on starting composition and Figs. 1 and 2 and Table 1.

In addition, samples whose initial compositions were in the single-phase field, were now multi-phased. This lead us to suspect Si loss during annealing.

Because of the relatively large uncertainty in the bulk chemical analysis, compared to the small atomic differences between individual samples and evaporative losses during annealing, EPMA was employed to help pinpoint the compositions of the T1 phase for samples which span the T1 stability field. Samples selected were based upon XRD results on the 48 hour anneals. Due to difficulties in quantitatively determining B content using EPMA [8] only $Mo_{1\alpha}$ and $Si_{k\alpha}$ lines were measured. The upper and lower limits of the boron concentrations were estimated using mass balance from the starting compositions and phase fractions.

It was suspected that the elemental standards would be inappropriate due to the high degree on covalent bonding in the T1 phase [10], which alters the efficiency of Mo X-ray generation. The intermetallic standards were the binary Mo_3Si and $MoSi_2$. The standards were synthesized using the binary eutectic compositions between T1 and Mo_3Si and T1 and $MoSi_2$.

Matrix corrected (ZAF) calculations were performed on all the Mo–Si–B samples using three different standard sets (Table 3). The Mo_3Si and $MoSi_2$ standards were also run as unknowns against pure Mo and Si as an internal check. Count rate variations on individual standards were within the range of the counting statistics, but the two silicide standards showed a systematic deviation from their nominal Si content when analyzed using pure Mo and Si as standards. The measured Si contents for Mo_3Si was 10 wt% Si (nominal 8.9 wt%), and 40.4 wt% for $MoSi_2$ (nominal 36.9 wt%). By contrast, all Mo analyses were within ± 0.3 wt% of the expected value. Totals were between 101.8 and 103.2 wt%, which further suggests that pure elemental standards over

estimates Si. To insure that the samples were homogeneous, multiple points (>24) were taken on the T1 phase. The overall standard deviation (σ^*) of a data set is typically around 0.6 at%. For n^* points in the data set, the confidence in the "true" value is then proportional to $\sigma^m = \sigma^*/\sqrt{n^*}$, which is <0.1 at%. The precision of the data is, therefore, of the order of 0.1–0.15 at%. This error range does not include any potential systematic error, since it is just determined from the distribution of the actual analyses. For all three standards the width of the binary Mo–Si phase field is 1.4 at%. The elemental standards grossly underestimate Mo content. The intermetallic standards are close, with Mo_3Si giving the highest Mo:Si ratio. This higher ratio is consistent with recent analysis of a single crystal of $Mo_{5+y}Si_{3-y}$ grown by zone refinement from the $Mo_{5+y}Si_{3-y}$-Mo_3Si binary [11]. While this gives greater credence to using the Mo_3Si standard, the difference in the Mo:Si using the two intermetallic standards is within the error of all the different analytical techniques.

The differences seen in the results using the two line compounds are assumed to be due to matrix effects. The relative absorptions are effected not only by the concentrations of the elements present, but also by the nature of the bonding in the crystal lattice. The Mo_3Si crystal structure contains more metal-metal bonds than $MoSi_2$. Although crystallographic orientation effects are minimal when compared to the effects of bonding within the crystal, the cubic structure of Mo_3Si should minimize orientation effects when compared to the tetragonal $MoSi_2$.

Table 2
Phases present after 48 h at 1800°C. Lattice parameters and unit cell volumes are for the T1 phase. The Mo:Si is for the T1 phase only and is based upon EMPA. B content is from starting composition

Sample ID	Major phase	Minor phase(s)	Mo/Si	B (at%)	Lattice parameters		
					a (Å)	c (Å)	Vol (Å)
A	T1		1.62	1.7			
B	T1		1.62	1.8			
C	T1			1.0			
D	T1	T2		1.7			
F	T1	T2 Mo_3Si		1.7	9.6315(2)	4.9019(1)	454.73(2)
I	T1	T2		2.0			
J	T1	T2	1.67	3.0			
K	T1	MoB		3.8			
O	T1	Mo_3Si		0.0	9.6533(4)	4.9135(2)	457.86(6)
P	T1			0.0	9.6546(3)	4.8879(2)	455.61(4)
Q	T1	Mo_3Si		1.0	9.6438(9)	4.9094(4)	456.(1)
R	T1	MoB		3.0			
T	T1	MoB	1.65	5.0			
U	T1			1.0			
V	T1			0.5			
W	T1	MoB		1.7			
X	T1	MoB	1.60	2.5	9.6471(2)	4.8834(1)	454.49(2)
Y	T1		1.62	2.0			
Z	T1			0.5			
λ	T1		1.67	1.0			
δ	T1			1.0			
ψ	T1			1.0			
Binary 1	T1	$MoSi_2$	1.60	0.0	9.6535(1)	4.8986(1)	456.50(1)
Binary 2	T1	Mo_3Si	1.70	0.0	9.6542(4)	4.9142(4)	458.03(6)

Table 3
A comparison of the compositions of the two boron-free end-members using different standards for ZAF correction of the EPMA data. Note that the width of the solid solution field is not changed

	Standards used					
Sample	Mo_3Si		$MoSi_2$		Elemental	
Atomic %	Mo (at%)	Si (at%)	Mo (at%)	Si (at%)	Mo (at%)	Si (at%)
Binary 1	61.5	38.5	60.9	39.1	58.6	41.4
Binary 2	62.9	37.1	62.3	37.7	60.1	39.9

Table 4
EPMA compositional analysis of Si and Mo content in the T1 phase of several samples. Boron values are from nominal starting compositions

Sample	No of points	Mo (wt%)	Si (wt%)	B (wt%)	Total	Mo (at%)	Si (at%)	Phases
X	52	83.9	15.4	0.4	99.2	61.5	38.5	T1 + MoB
λ	23	84.4	14.8	0.2	99.4	62.5	37.5	T1
Y	55	83.2	15.1	0.3	98.5	61.8	38.2	T1
T	98	84.8	15.1	0.8	99.9	62.2	37.8	T1 + MoB
T	67	84.3	15.0	0.8	99.3	62.2	37.8	T1 + MoB
B	50	83.6	15.1	0.3	99.0	61.9	38.1	T1
J	78	84.0	14.7	0.5	98.7	62.5	37.5	T1 + T2
A	75	83.7	15.1	0.3	99.1	61.8	38.2	T1

The analysis of the Mo:Si in B containing T1 phase in select samples using the Mo_3Si standard are given in Table 4. Sample T was tested twice to check the precision of the data, but this does not take into account any systematic errors that could occur. A large number of data points were taken on multiple grains (> 50 points) and the variance was determined for each sample. In all cases the variance was quite low, indicating that homogeneity was achieved after annealing the samples for 48 h at 1800°C. In addition, the lower limit of Mo:Si ratio increases for samples with nominally increasing B. This is in qualitative agreement with the XRD results suggesting that B is substituting on the Si lattice site (Table 2).

The differences seen in the compositions calculated using mass balance and those obtained using EPMA are generally within 0.5 at% of one another. The compositions in Table 4 tend to be slightly higher in Mo than those calculated from mass balance of the arc melt buttons. This discrepancy could be attributed to the formation of SiO_2 inclusions during powder processing which would decrease the silicon content of the T1 grains. The presence of SiO_2 was confirmed by optical microscopy. Also, the high temperature used during annealing could also be responsible for a shift in the compositions towards the molybdenum rich side due to the high vapor pressure of silicon at 1800°C.

While B was not specifically analyzed for, both the XRD results, showing a decrease in the lattice parameters with nominal increase in B (Fig. 7), and the bulk chemistry on single phase samples with little (< 2 vol %) glassy phase all support B incorporation into the structure. Since the EPMA also shows that the solubility range spans the ideal stoichiometric composition, this would suggest that the crystal structure can either accommodate the nonstoichiometry through vacancies or substitutions on both Si and Mo sites. The lattice volume increases with increasing Mo:Si in samples without B suggests that hypostoichiometric T1 forms by Mo vacancies. This would also account for the small volume increase with B additions if the B substituted into the Mo vacancies. The Reitveld fits to the XRD data for the hypostoichiometric samples were improved slightly when the Mo 4b site was fitted for a fractional occupancy (Table 5). In the hyperstoichiometric T1, there is a relatively large B effect on the cell volume for nearly constant Mo:Si (Fig. 7). This suggested that Si replaces Mo while B replaces Si. The most likely candidate for direct substitution of B for Si is the 4a (0,0,1/4) site which Si occupies in both the T1 and T2 structures. Also note that there is an excellent agreement between the occupations determined by XRD and EMPA results for the binary alloys (Table 5).

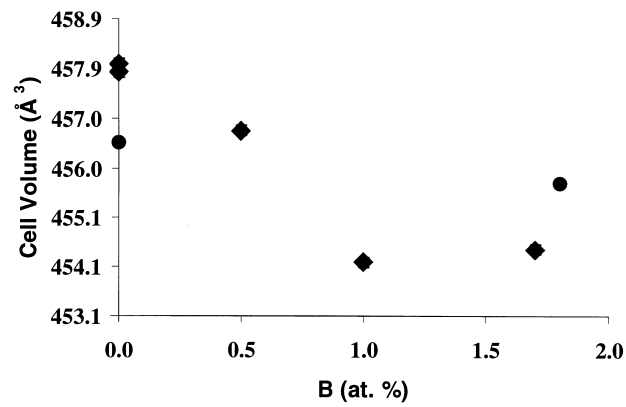

Fig. 7. Change in lattice volume as a function of B concentration (T1 along the T1-$MoSi_2$ (○) and along the T1-Mo_3Si (◆) boundary).

4. Summary

Using XRD, chemical analysis, and EPMA it was determined that the maximum level of boron solubility in T1 is close to 2 at%. The boron solubility reaches a maximum near the center of the T1 homogeneity range. This region of solubility appears to be much smaller than first reported by Nowotny. However, the phase assemblages shown on the Nowotny diagram appear to hold true at 1800°C.

Table 5
Rietveld fits for select samples of T1 without B. The space group is I4/mcm with Mo(1) (0, 1/2, 1/4), Mo(2) (x, y, 0), Si(1) (0, 0, 1/4) and Si(2) (x, y, 0). The calculated Mo:Si ratios agree well with EMPA results

Sample	Mo(2)		Si(2)		Fractional occupancies		Mo:Si	
	x	y	x	y	Mo(1)	Si(2)	EMPA	XRD
L	0.0768	0.2230	0.1681	0.6681	0.913	1.00	1.60	1.59
M	0.0767	0.2232	0.1664	0.6664	0.910	1.00		1.59
N	0.0769	0.2225	0.1685	0.6685	1.00	0.931		1.71
O	0.0770	0.2230	0.1686	0.6686	1.00	0.966	1.70	1.70

Fig. 2 shows the experimentally determined ternary diagram in the T1 region at 1800°C. The dashed boundary corresponds to the T1 region shown on the Nowotny 1600°C diagram. Our work was carried out at 1800°C, rather than 1600°C, in an effort to more closely simulate operating temperatures for these materials. Also, using longer annealing times on powder processed samples at a higher temperature assured us that we were reaching equilibrium.

Long term annealing of powder processed samples not only appeared to reach thermodynamic equilibrium, but also showed that the T1 phase is not metastable. Some samples that were annealed at 1800°C for as long as 92 h stayed single phase T1. There was no noticeable difference in lattice parameters between the 48 h and the 92 h samples. The need to powder process samples after arc-melting underscores the sluggish diffusion in this system. It is doubtful that annealed cast samples would ever reach thermodynamic equilibrium in any reasonable time frame except at very high homologous temperatures.

The solubility range for boron into $Mo_{5+y}Si_{3-y}$, however, appears to be under 2 at% within the homogeneity range for single phase $Mo_{5+y}Si_{3-y}$. Lattice parameter values are given only for the T1 phase in each of the samples, and have a typical error range of ± 0.001Å as read from the numerical fit using the G.S.A.S. program. The contraction in the unit cell volume for the boron doped samples indicates that the boron atoms are either making a direct substitution for silicon in the lattice or filling in for silicon vacancies.

Acknowledgements

The authors would like to thank A. Kracher for his help with the EPMA data collection and analysis. Ames Laboratory is operated by the U.S. Department of Energy by Iowa State University under contract number W-7405-ENG-82. This research was supported by the Office of Basic Energy Science, Materials Science Division.

References

[1] Meyer M, Kramer M, Akinc M. Adv Mat 1996;8:85.
[2] Meyer M, Kramer M, Akinc M. Intermet 1996;4:273–81.
[3] Thom A, Meyer M, Williams J, Akinc M. In: Srivatsan T, Moore J. editors. Processing and fabrication of advanced materials IV. 139.
[4] Nowotny H, Dimakopoulou E, Kudielka H. Mh Chem 1957;2:180.
[5] Nowotny H, Parthe E, Kieffer R, Benesovsky F. Mh Chem 1954;1:255.
[6] Nowotny H, Lux B, Kudielka H. Mh Chem 1956;3:447.
[7] Larson AC, Von Dreele RB. General structure analysis system. Los Alamos, NM: Los Alamos National Laboratory, 1994.
[8] Nunes SR, Perepezko J. Structural intermetallics. In: Nathal MV, Darolia R, Liu CT, Martin PL, Miracle DB, Wagner R, Yamaguchi M, editors. Minerals, metals and materials society. 1997, p. 831–839.
[9] Schneible JH, Liu CT, Easton DS, Carmichael CA. Mat Sci Eng 1999;A261:78.
[10] Fu CL, Wang X, Ye YY, Ho KM. Intermet 1998;7:1.
[11] Chu F, Thoma DJ. Processing and properties of Mo5Si3 single crystals. In: Bray D, editor. 22nd Conference on Composites, Advances Ceramics and Structures. ACERS, 1998. p. 413.